

SCIENTIFIC REPORTS



OPEN

Electro-mechanical light modulator based on controlling the interaction of light with a metasurface

Pablo Cencillo-Abad¹, Jun-Yu Ou¹, Eric Plum¹ & Nikolay I. Zheludev^{1,2}

We demonstrate a reflective light modulator, a dynamic Salisbury screen where modulation of light is achieved by moving a thin metamaterial absorber to control its interaction with the standing wave formed by the incident wave and its reflection on a mirror. Electrostatic actuation of the plasmonic metamaterial absorber's position leads to a dynamic change of the Salisbury screen's spectral response and 50% modulation of the reflected light intensity in the near infrared part of the spectrum. The proposed approach can also be used with other metasurfaces to control the changes they impose on the polarization, intensity, phase, spectrum and directional distribution of reflected light.

From their beginnings as microwave frequency selective surfaces¹, metasurfaces have developed into a diverse branch of nanophotonics². Such essentially planar arrays of resonators of sub-wavelength size are being used as spectral filters, wave plates³, polarizers^{4,5} and — based on spatially varying resonators — for redirection^{6–8} and focusing⁹ of light as well as holography^{10,11}. Dynamic control over such structures has been achieved by modifying the materials that make up a metasurface, e.g. using phase transitions^{12–14} or optical nonlinearities^{15,16}, by nanomechanical rearrangement of the array of coupled resonators^{17,18}, and by controlling the metasurface excitation with counterpropagating coherent beams of light¹⁹. However, these approaches rely on special materials and operating conditions (e.g. temperature, intensity); or complex and fragile nanostructures; or extremely stable interferometric setups.

Here we use nanoelectromechanical actuation to control metasurface excitation in a robust way that is compatible with ambient conditions. We place a plasmonic metasurface absorber of nanoscale thickness a few microns in front of a mirror. Using electrostatic forces, we move the metasurface between positions of constructive interference and positions of destructive interference to control the light-metasurface interaction, resulting in high-contrast modulation of absorption and significant spectral shifts of the structure's absorption resonances. The combination of a metasurface with a backing mirror is known as Salisbury screen^{1,20,21} and has been used previously to control optomechanical resonances²², to realize a mid-infrared electro-optical switch²³ and to enhance metasurface performance, e.g. to achieve phase gradient metasurfaces with high efficiency^{24,25} as well as handedness-maintaining²⁶ and handedness-inverting²⁷ mirrors for a single circular polarization. Here we highlight that dynamic control over the spacing of a metasurface of substantially sub-wavelength thickness and a backing mirror provides an effective solution for tuning, modulating and switching the various optical functionalities metasurfaces can provide.

Any material of substantially sub-wavelength thickness may be placed at a node or anti-node of a standing wave formed by coherent counterpropagating waves. At an electric field node of the standing wave, there is no electric field that could interact with the material and therefore the electric light-matter interaction vanishes. In contrast, at an electric field anti-node, the electric field amplitude doubles due to constructive interference, leading to enhancement of the electric light-matter interaction. Thus, the light-matter interaction may be controlled by modulating the relative position of standing wave and material. Such coherent control of light with light has been exploited to control absorption of light from almost 0% to almost 100%¹⁹, to control the propagation direction of light interacting with phase gradient metasurfaces²⁸ and to control polarization of light interacting with anisotropic metasurfaces²⁹, with applications including all-optical logic gates³⁰ and parallel information processing³¹. These works have been based on meter-scale laser Mach-Zhender interferometers, which had to be stable on a length-scale of few nanometers as nodes and anti-nodes are separated by a quarter of the wavelength. Our

¹Optoelectronics Research Centre and Centre for Photonic Metamaterials, University of Southampton, Highfield, Southampton, SO17 1BJ, UK. ²Centre for Disruptive Photonic Technologies, School of Physical and Mathematical Sciences and The Photonics Institute, Nanyang Technological University, Singapore, 637371, Singapore. Correspondence and requests for materials should be addressed to E.P. (email: erp@orc.soton.ac.uk)

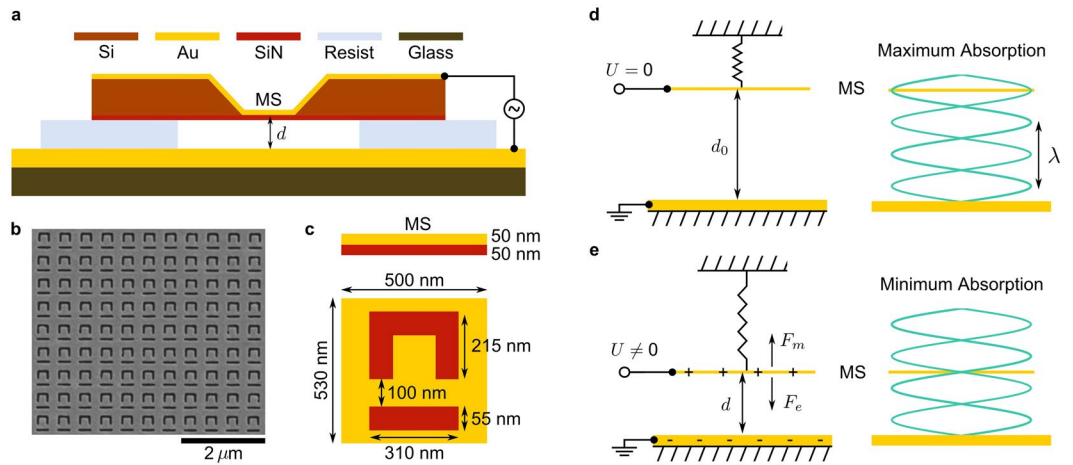


Figure 1. Electrostatic control of metasurface excitation. **(a)** Schematic cross-section of the metadvice consisting of a nanostructured gold-coated silicon nitride membrane separated from a gold-coated glass substrate by a resist spacer layer. **(b)** Scanning electron micrograph of a fragment of the lossy metasurface (MS) consisting of asymmetrically split ring apertures in 50 nm of gold on 50 nm of silicon nitride and **(c)** its cross-section and unit cell. **(d,e)** Operating principle of the device that is actuated by application of a voltage U leading to an electrostatic force F_e balanced by an elastic restoring force F_m . The resulting change of the metasurface-to-mirror distance d translates the metasurface between positions of **(d)** constructive interference corresponding to enhanced light-metasurface interaction and **(e)** destructive interference corresponding to suppressed light-metasurface interaction.

approach avoids such challenges by shrinking the interferometer size by 5–6 orders of magnitude. By placing the metasurface in the standing wave that forms in front of a mirror we create a Fabry-Perot microcavity of variable length that controls the light-metasurface interaction.

Results and Discussion

The metadvice consists of an electrostatically actuated metasurface that forms a Fabry-Perot microcavity of variable length with a gold mirror as illustrated by Fig. 1. The metasurface is an array of asymmetrically split ring apertures in a 50-nm-thick gold layer supported by a 50-nm-thick silicon nitride membrane, see Methods for details. Asymmetrically split ring apertures were chosen as they are well-studied³² and known to provide coherent perfect absorption¹⁹. Application of an electrical voltage U to the gold layers of the device leads to charge accumulation in the elastic metamaterial and the gold mirror in a way that is similar to a parallel plate capacitor. The resulting electrostatic force F_e bends the nanomembrane metamaterial to an equilibrium point where it is balanced by the mechanical restoring force F_m of the elastic structure. Thus, the applied voltage U controls the metasurface-to-mirror distance d (cavity length). We note that the electrostatic force grows infinite as the distance approaches zero, while the elastic force scales linearly with the deformation, leading to unstable behaviour for sufficiently large U . Indeed, a pull-in voltage U_p can be defined above which the electrostatic force cannot be compensated by elastic forces resulting in membrane-to-mirror stiction and device failure. Following³³, the relationship between applied voltage and resulting metamaterial displacement $\Delta d = d_0 - d$ (cavity length change) is given by

$$U^2 = \frac{27}{4} \frac{\Delta d}{d_0} \left(1 - \frac{\Delta d}{d_0} \right)^2 U_p^2, \quad (1)$$

where d_0 is the metasurface-to-mirror distance without applied voltage and $\Delta d_p = \frac{1}{3} d_0$ corresponds to the metasurface displacement at the pull-in voltage, i.e. the displacement at which device failure is expected. For small displacements, $\Delta d \ll d_0$, the displacement is proportional to the square of the applied voltage,

$$\Delta d \simeq \frac{4}{27} \frac{U^2}{U_p^2} d_0. \quad (2)$$

The optical properties of the metadvice are most easily understood by considering the standing wave that forms in front of a mirror. For a given wavelength of light, the metasurface may be placed at an anti-node or node of the standing wave, depending on the voltage applied to the metadvice, see Fig. 1d,e. At an electric field anti-node, light will interact strongly with the lossy metasurface resulting in large absorption that can reach 100% (coherent perfect absorption). In contrast, absence of electric field at a node will lead to weak light-metasurface interaction with 0% absorption in the ideal case (coherent perfect transparency).

An accurate description of the metadvice's optical properties must consider the characteristics of the Fabry-Perot cavity formed by metasurface and mirror as well as the optical response of the metasurface itself.

Throughout this work we consider linearly polarized light with the electric field oriented parallel to the symmetry axis of the metamaterial pattern.

The optical response of a Fabry-Perot cavity formed by a partially transparent interface and a mirror is determined by multiple reflections of light and its absorption A and reflectivity R are given by

$$A(\lambda) = 1 - R(\lambda) = 1 - \left| r_o + \frac{mt^2 e^{-i4\pi d/\lambda}}{1 - mr_i e^{-i4\pi d/\lambda}} \right|^2 \quad (3)$$

where $r_o(\lambda)$ and $r_i(\lambda)$ are the complex Fresnel reflection coefficients for illumination of the partially transparent interface from outside and inside the cavity, $t(\lambda)$ is its transmission coefficient, $m(\lambda) \simeq -1$ is the mirror's reflection coefficient and $2\pi d/\lambda$ is the phase accumulated during propagation of the wave of wavelength λ from interface to mirror²⁴. In the cases considered here, absorption by the mirror is small and absorption of the cavity is therefore dominated by absorption in the partially transparent interface, which is controlled by constructive/destructive interference of incident and multiply reflected waves on the interface.

While equation (3) implies interference effects for any cavity length, observation of the cavity resonances with good visibility requires the cavity length d to be small compared to the coherence length $l_c \simeq c/\Delta f$, where c is the speed of light and Δf is the spectral bandwidth in terms of frequency. For larger cavity lengths, interference effects average out over the detected spectral band which will contain wavelengths experiencing both constructive and destructive interference on the lossy interface. Notably, for a narrow-band light source detected with a broadband detector Δf is the spectral bandwidth of the light source, while for a broadband light source detected with a narrowband detector (or a spectrometer) Δf is the spectral bandwidth (or resolution) of the detector. Assuming linear superposition of light at different wavelengths, this effect of temporal coherence on the measured absorption A_M can be described by

$$A_M = \int P(\lambda)A(\lambda)d\lambda, \quad (4)$$

where $P(\lambda)$ is the normalized product of spectral power distribution and detector sensitivity. For measurements with a spectrometer this applies to each spectral bin and for our experimental wavelength range of 950 nm–2000 nm with a spectral resolution of 7 nm the coherence length ranges from 136 μm to 286 μm .

In order to disentangle the effects of Fabry-Perot cavity and metasurface, we will first consider a Fabry-Perot cavity formed by a gold mirror and an ideal lossy beam splitter in the incoherent and coherent regimes, characterized by the cavity length being much larger and much smaller than the coherence length, respectively. An ideal lossy beam splitter exhibits the largest possible absorption for planar metasurfaces, which is 50% of a single beam illuminating one side of the metasurface³⁵, and its Fresnel reflection and transmission coefficients are $r_{o,i} = -0.5$ and $t = +0.5$. As illustrated by Fig. 2a, in the coherent case, the Fabry-Perot cavity exhibits alternating absorption maxima and minima, corresponding to constructive and destructive interference of light on the lossy beam splitter, respectively, while no interference effects can be seen in the incoherent case. Figure 2b shows the simulated absorption spectrum of the metasurface, which has absorption resonances at wavelengths of about 1024 nm and 1389 nm, see Methods for details on numerical modelling. Figure 2c shows the absorption spectrum of the whole metadvice consisting of metasurface and mirror as a function of the cavity length d . For cavity lengths that are small compared to the coherence length, the absorption spectrum of the metadvice corresponds to Fabry-Perot resonances with an envelope that resembles the absorption spectrum of the metamaterial. Negligible light-metasurface interaction due to destructive interference of light on the metasurface when the cavity length is a multiple of $\lambda/2$ is apparent as absorption minima corresponding to dark blue straight lines on the colour map. Indeed, for any ideal planar metasurface ($t = r_{o,i} + 1$) and an ideal mirror ($m = -1$) absorption according to equation (3) is zero in this case. In contrast to the absorption minima, both spectral position and amplitude of the absorption maxima depend on the optical properties of the metasurface in addition to the cavity length. As the achievable maximum displacement Δd_p is proportional to the cavity length, longer cavities enable a larger dynamic range of absorption modulation, provided that the cavity length remains small compared to the coherence length. However, as the voltage required to achieve a given displacement is also proportional to the cavity length, longer cavities imply larger actuation voltages. The spectral separation of the Fabry-Perot resonances decreases with increasing cavity length, preventing their detection when the cavity length becomes half of the coherence length as their spectral separation equals the spectral resolution of the spectrometer in this case. For our spectral resolution of 7 nm, the coherence length is 140 μm at about 1000 nm wavelength, causing the Fabry-Perot resonances at this wavelength to vanish for a cavity length of 70 μm , while Fabry-Perot resonances at longer wavelengths remain visible as they correspond to longer coherence lengths, see Fig. 2c. For large cavity lengths, the Fabry-Perot resonances cannot be resolved resulting in a metadvice absorption spectrum that is similar to that of the metasurface.

Figure 3a shows absorption spectra of the metadvice measured with 7 nm spectral resolution for applied voltages of 0 V and 20 V (see Methods) alongside numerical fits based on equation (4), where the cavity length d is the only fitting parameter. The spectra show absorption maxima and minima corresponding to enhanced and suppressed metasurface excitation due to constructive and destructive interference, respectively. The largest absorption is found near the metasurface resonances and the spectral positions of measured and simulated absorption maxima and minima are in close agreement. Gallium implantation during focused ion beam milling of the metasurface, nanofabrication inaccuracies, a small variation of the cavity length across the metasurface area and focused illumination with a 0.28 numerical aperture objective contribute to reduced contrast in the experimental absorption spectra. Application of 20 V reduces the cavity length from $d_0 = 5485$ nm to 5406 nm, that is by 79 nm. This cavity length change of 1.44% leads to a blue-shift of the metadvice's spectral response of the same

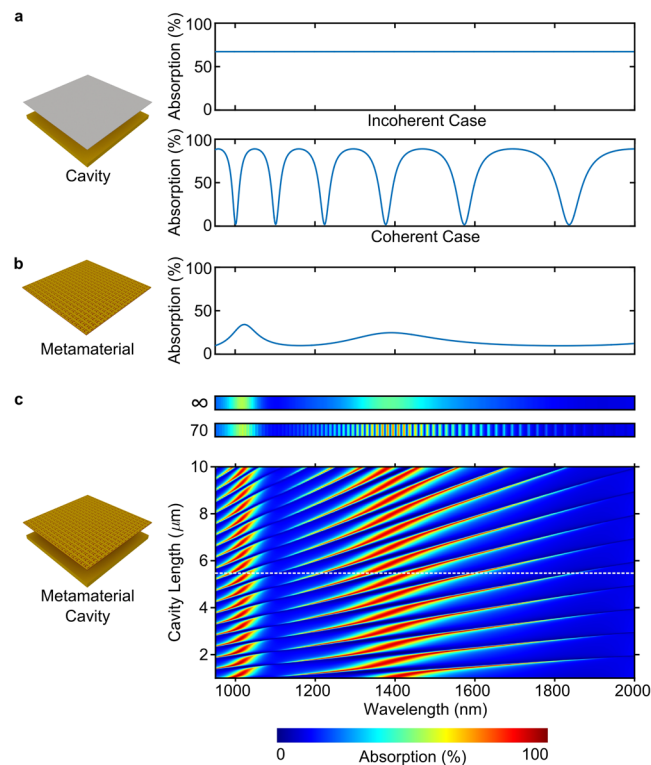


Figure 2. Interactions between Fabry-Perot cavity and metasurface. **(a)** Absorption of a Fabry-Perot cavity formed by a gold mirror and an ideal lossy beam splitter of infinitesimal thickness in the limiting cases corresponding to cavity lengths much larger (top) and much smaller (bottom) than the coherence length. The coherent case assumes a cavity length of $d_0 = 5485$ nm. **(b)** Absorption spectrum of the metasurface. **(c)** Absorption spectrum of the metadvice consisting of metasurface and gold mirror as a function of cavity length d assuming 7 nm detector bandwidth. The experimental cavity length $d_0 = 5485$ nm is indicated by a dashed line. All results shown in this figure are simulations.

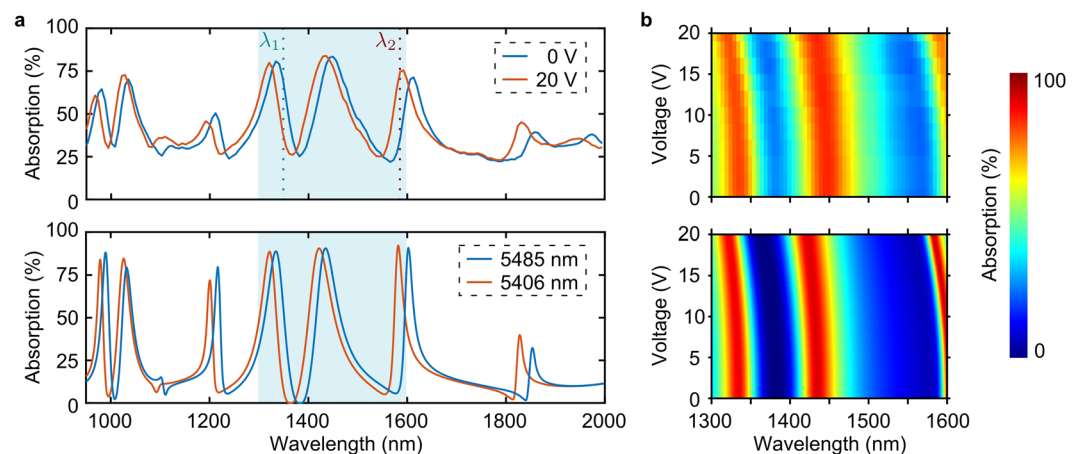


Figure 3. Electric tuning of absorption bands. **(a)** Absorption spectra measured with voltages U of 0 V and 20 V applied to the metadvice (top) and best fit theoretical absorption corresponding to metasurface-to-mirror spacings d of 5485 nm and 5406 nm based on equation (4) assuming the experimental detector bandwidth of 7 nm (bottom). **(b)** Experimental and theoretical absorption spectra as a function of voltage U , where theoretical spectra are calculated as above for cavity lengths $d = d_0 - \Delta d$ given by equation (1) with $U_p = 66$ V and $d_0 = 5485$ nm.

magnitude, i.e. a 20 nm blue-shift around 1400 nm wavelength. The measured and simulated voltage-dependence of absorption is given by Fig. 3b for the spectral range of highest contrast and the corresponding metasurface displacements that were determined by fitting the experimental absorption spectra are shown by Fig. 4a. Both

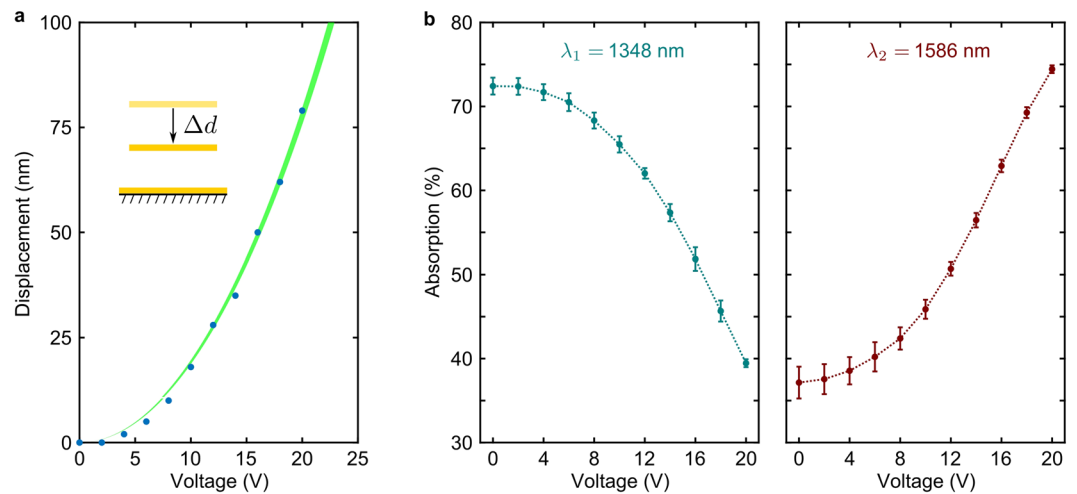


Figure 4. Electric control over metasurface deformation and absorption. (a) Metasurface displacement Δd as a function of voltage U , where the data points were obtained by fitting the experimental spectra as in Fig. 3a and the green curve corresponds to equation (1) with $U_p = 66$ V and $d_0 = 5485$ nm, with line width indicating the 95% confidence interval of the fit. (b) Tuning of absorption at $\lambda_1 = 1348$ nm and $\lambda_2 = 1586$ nm by gradual voltage application, where dotted lines serve as an eye guide.

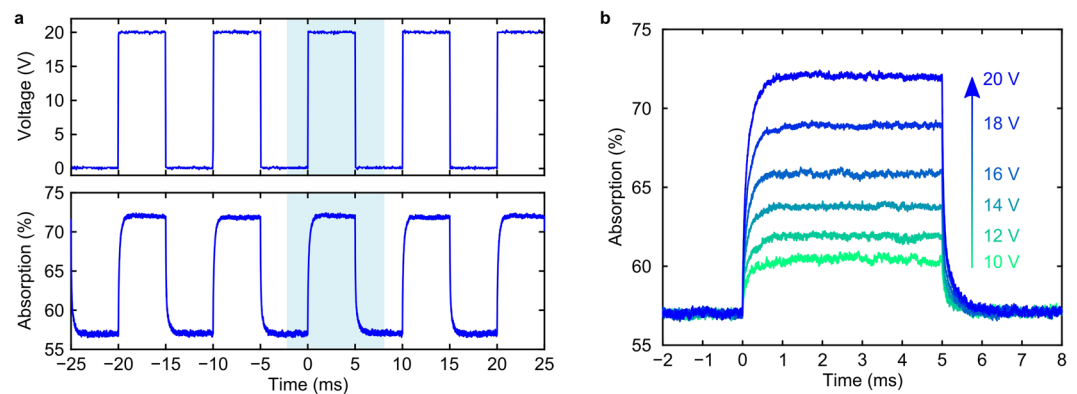


Figure 5. Modulating metasurface absorption. (a) Square modulation of the applied voltage U between 0 V and a peak voltage of 20 V (top) at 100 Hz and the resulting absorption modulation at a wavelength of 1310 nm (bottom). (b) One cycle of modulation for peak voltages from 10 V to 20 V in steps of 2 V.

spectral shift and metasurface displacement are proportional to the square of the applied voltage within our experimental range of voltages. The voltage-dependence of the metasurface displacement closely follows equation (1) with a pull-in voltage of $U_p = 66$ V corresponding to a maximum displacement of $\Delta d_p \approx 1.8 \mu\text{m}$. Thus, our cavity length of $d_0 = 5485$ nm is big enough to allow a large dynamic range of modulation and sufficiently small to operate the metasurface with reasonable actuation voltages within the coherent regime. Throughout our experiments, we limited the applied voltage to a maximum of 20 V, which is well below the pull-in voltage and thus avoids any risk of electrical damage, while being sufficient for metasurface operation and characterization.

The voltage-induced spectral shift of the metasurface absorption spectrum leads to large intensity changes at specific wavelengths, which may be exploited for tuning and modulation. This is illustrated by Fig. 4b for selected wavelengths of $\lambda_1 = 1348$ nm and $\lambda_2 = 1586$ nm, where absorption and reflection can be changed by a factor of two. Gradual changes of the applied voltage between 0 V and 20 V lead to gradual changes in absorption. On cycling of the applied voltage, the values were reproduced within 2% in terms of absolute absorption.

The dynamic switching behaviour of the metasurface was measured by detecting the structure's reflectivity at 1310 nm wavelength while modulating the actuation voltage (see Methods). Figure 5 shows how the metasurface absorption changes in response to application of a step-like voltage. Upon voltage application and withdrawal, the absorption — and thus the metasurface-to-mirror spacing — approaches its new equilibrium position exponentially with a characteristic time constant of about $150 \mu\text{s}$. Thus, the switching behaviour of the metasurface is consistent with an overdamped harmonic oscillator, where the air surrounding the metasurface is a source of damping. In general, the temporal resolution of nanomembrane metamaterials is controlled by the dimensions of the metasurface membrane, the density and Young's modulus of the constituent materials and the damping

effect of the surrounding atmosphere¹⁷. Faster modulation can be achieved by operating a metadvice based on a smaller membrane in a low pressure environment. Like metasurface displacement and slow tuning of metadvice absorption, as shown in Fig. 4, also the magnitude of the observed absorption modulation is approximately proportional to the square of the applied voltage.

The optical damage threshold of the metadvice due to melting of the gold nanostructure is controlled by heat transport away from the metasurface by thermal conduction along the metasurface membrane and convection by the surrounding atmosphere. We did not observe any thermal issues in our experiments conducted at sub-milliwatt power levels, however, based on the thermal properties of similar plasmonic nanomembrane metamaterials³⁶ we expect that our metadvice can tolerate illumination with at least several milliwatts.

Absorption of our metadvice is a measure of metasurface excitation. Therefore, we argue that our method can be employed to control the light-matter interaction of any metasurface or functional film of substantially sub-wavelength thickness in a reliable and repeatable way at ambient conditions. For example, phase gradient metasurfaces for holography, redirection and focusing of light may be turned on and off, while anisotropic and chiral metasurfaces may become polarization modulators. Metasurfaces or thin films can also be separated into smaller elastic sections with individual electrical contacts, e.g. strips, in order to achieve dynamic spatial control over their functionality³⁷. It has been demonstrated numerically, that reconfigurable elements of sub-wavelength spacing can deliver effectively continuous spatial control over the intensity of light³⁴.

Conclusion

In summary, we demonstrate dynamic control over metasurface excitation by assembling a Fabry-Perot microcavity from a gold mirror and an elastic metasurface that is actuated by electrostatic forces. The metadvice acts as an electrically controlled spectral filter and intensity modulator achieving an intensity contrast of two in our experiments. While our metadvice modulates absorption of light, we argue that our method may be used to control any of the diverse optical functionalities that metasurfaces and films of substantially sub-wavelength thickness can provide.

Methods

Metadvice fabrication. The metadvice was fabricated starting with a commercially available $500 \times 500 \mu\text{m}^2$ silicon nitride membrane of 50 nm thickness that is supported by a $5 \times 5 \text{mm}^2$ silicon frame (Norcada Inc) and a glass substrate, see Fig. 1. The mirror was fabricated by coating the glass substrate with 200 nm of gold using thermal evaporation. Using the same technique, the membrane was coated with a 50-nm-thick gold layer that was then perforated by focused ion beam milling to create the metasurface, an array of asymmetrically split ring apertures. The metasurface has an overall size of $30 \times 30 \mu\text{m}^2$ with a $500 \times 530 \text{nm}^2$ unit cell. Photolithography resist (S1813) was used as a spacer on top of the gold mirror. A central groove of about 1 mm width was exposed and developed to generate the gap of the resonant cavity. The metadvice was finally assembled by placing the membrane in front of the mirror, taking care to align the groove with the membrane window.

Simulations. Numerical modelling uses a Drude-Lorentz model with 3 oscillators for the electric permittivity of gold³⁸ and a constant permittivity of 4.0 for silicon nitride. The optical properties of the metasurface were simulated for normal incidence illumination by a plane wave considering a single unit cell with periodic boundary conditions using finite element method modelling (COMSOL Multiphysics 4.4) in three dimensions.

Experimental metadvice characterization. Absorption spectra of the metadvice — which cannot transmit light — were determined from its reflectivity spectra that were measured with applied voltages between 0 V and 20 V using a microspectrophotometer (CRAIC Technologies) with a halogen light source and 7 nm spectral resolution, see Figs 3 and 4b. The dynamic switching behaviour of the metadvice was measured by detecting the reflection of a 1310 nm CW laser using a photodetector and an oscilloscope, while modulating the actuation voltage with a function generator, see Fig. 5.

Data Availability. The data from this paper can be obtained from the University of Southampton ePrints research repository: <http://doi.org/10.5258/SOTON/D0044>.

References

- Munk, B. A. *Frequency Selective Surfaces: Theory and Design* (Wiley-Interscience, 2000), 1st edn.
- Urbas, A. M. *et al.* Roadmap on optical metamaterials. *J. Opt.* **18**, 093005 (2016).
- Peralta, X. G. *et al.* Metamaterials for THz polarimetric devices. *Opt. Express* **17**, 773 (2009).
- Tamada, H., Doumuki, T., Yamaguchi, T. & Matsumoto, S. A wire-grid polarizer using the s-polarization resonance effect at the 0.8- μm -wavelength band. *Opt. Lett.* **22**, 419 (1997).
- Ahn, S. W. *et al.* Fabrication of a 50 nm half-pitch wire grid polarizer using nanoimprint lithography. *Nanotechnology* **16**, 1874 (2005).
- Yu, N. F. *et al.* Light propagation with phase discontinuities: generalized laws of reflection and refraction. *Science* **334**, 333–337 (2011).
- Roy, T., Nikolaenko, A. E. & Rogers, E. T. A meta-diffraction-grating for visible light. *J. Opt.* **15**, 85101 (2013).
- Veksler, D., Maguid, E., Shitrit, N., Ozeri, D. & Kleiner, V. Multiple wavefront shaping by metasurface based on mixed random antenna groups. *ACS Photonics* **2**, 661–667 (2015).
- Ni, X. J., Ishii, S., Kildishev, A. V. & Shalaev, V. M. Ultra-thin, planar, babinet-inverted plasmonic metalenses. *Light. Sci. Appl.* **2**, e72 (2013).
- Walther, B., Helgert, C., Rockstuhl, C., Setzpfandt, F. & Eilenberger, F. Spatial and spectral light shaping with metamaterials. *Adv. Mater.* **24**, 6300–6304 (2012).
- Wang, Q. *et al.* Polarization and frequency multiplexed terahertz metaholography. *Adv. Opt. Mater.* **5**, 1700277 (2017).
- Driscoll, T. *et al.* Memory metamaterials. *Science* **325**, 1518–1521 (2009).
- Sámson, Z. L. *et al.* Metamaterial electro-optic switch of nanoscale thickness. *Appl. Phys. Lett.* **96**, 143105 (2010).

14. Wang, Q. *et al.* Optically reconfigurable metasurfaces and photonic devices based on phase change materials. *Nature Photon.* **10**, 60–65 (2016).
15. Cho, D. J. *et al.* Ultrafast modulation of optical metamaterials. *Opt. Express* **17**, 17652–17657 (2009).
16. Dani, K. M. *et al.* Subpicosecond optical switching with a negative index metamaterial. *Nano Lett.* **9**, 3565–3569 (2009).
17. Zheludev, N. I. & Plum, E. Reconfigurable nanomechanical photonic metamaterials. *Nat. Nanotechnol.* **11**, 16–22 (2016).
18. Ou, J. Y., Plum, E., Zhang, J. & Zheludev, N. I. An electromechanically reconfigurable plasmonic metamaterial operating in the near-infrared. *Nat. Nanotechnol.* **8**, 252–255 (2013).
19. Zhang, J., MacDonald, K. F. & Zheludev, N. I. Controlling light-with-light without nonlinearity. *Light Sci. Appl.* **1**, e18 (2012).
20. Fante, R. L. & McCormack, M. T. Reflection properties of the salisbury screen. *IEEE Trans. Antennas. Propag.* **36**, 1443–1454 (1988).
21. Engheta, N. Thin absorbing screens using metamaterial surfaces. *Antennas and Propagation Society International Symposium* **2**, 392–395 (2002).
22. Zhu, H., Yi, F. & Cubukcu, E. Plasmonic metamaterial absorber for broadband manipulation of mechanical resonances. *Nature Photon.* **10**, 709–714 (2016).
23. Liu, X. & Padilla, W. J. Dynamic manipulation of infrared radiation with MEMS metamaterials. *Adv. Opt. Mater.* **1**, 559–562 (2013).
24. Sun, S. L. *et al.* High-efficiency broadband anomalous reflection by gradient meta-surfaces. *Nano Lett.* **12**, 6223–6229 (2012).
25. Chen, W. T. *et al.* High-efficiency broadband meta-hologram with polarization-controlled dual images. *Nano Lett.* **14**, 225–230 (2014).
26. Plum, E. & Zheludev, N. I. Chiral mirrors. *Appl. Phys. Lett.* **106**, 221901 (2015).
27. Plum, E. Extrinsic chirality: Tunable optically active reflectors and perfect absorbers. *Appl. Phys. Lett.* **108**, 241905 (2016).
28. Shi, J. *et al.* Coherent control of snell's law at metasurfaces. *Opt. Express* **22**, 21051–21060 (2014).
29. Mousavi, S. A., Plum, E., Shi, J. & Zheludev, N. I. Coherent control of optical polarization effects in metamaterials. *Sci. Rep.* **5**, 8977 (2015).
30. Fang, X., MacDonald, K. F. & Zheludev, N. I. Controlling light with light using coherent metadevices: all-optical transistor, sumulator and inverter. *Light Sci. Appl.* **4**, e292 (2015).
31. Papaioannou, M., Plum, E., Valente, J., Rogers, E. T. F. & Zheludev, N. I. All-optical multichannel logic based on coherent perfect absorption in a plasmonic metamaterial. *APL Photonics* **1**, 090801 (2016).
32. Plum, E. *et al.* A combinatorial approach to metamaterials discovery. *J. Opt.* **13**, 055102 (2011).
33. Kaajakari, V. *Practical MEMS* (Small Gear Pub., 2009).
34. Cencillo-Abad, P., Zheludev, N. I. & Plum, E. Metadevice for intensity modulation with sub-wavelength spatial resolution. *Sci. Rep.* **6**, 37109 (2016).
35. Thongrattanasiri, S., Koppens, F. H. L. & de Abajo, F. J. G. Complete optical absorption in periodically patterned graphene. *Phys. Rev. Lett.* **108**, 047401 (2012).
36. Ou, J. Y., Plum, E., Zhang, J. & Zheludev, N. I. Giant nonlinearity of an optically reconfigurable plasmonic metamaterial. *Adv. Mater.* **28**, 729–733 (2016).
37. Cencillo-Abad, P., Ou, J. Y., Plum, E., Valente, J. & Zheludev, N. I. Random access actuation of nanowire grid metamaterial. *Nanotechnology* **27**, 485206 (2016).
38. Liu, Z. *et al.* Plasmonic nanoantenna arrays for the visible. *Metamaterials* **2**, 45–51 (2008).

Acknowledgements

This work is supported by the MOE Singapore (grant MOE2011-T3-1-005) and the UK's Engineering and Physical Sciences Research Council (grants EP/G060363/1 and EP/M009122/1). The authors acknowledge the use of the IRIDIS High Performance Computing Facility, and associated support services at the University of Southampton, in the completion of this work.

Author Contributions

P.C.A. and J.Y.O. carried out the nanofabrication, experiments, simulations and performed the data analysis. P.C.A. and E.P. drafted the manuscript. J.Y.O., E.P. and N.I.Z. supervised the work and all authors read and approved the manuscript.

Additional Information

Competing Interests: The authors declare that they have no competing interests.

Publisher's note: Springer Nature remains neutral with regard to jurisdictional claims in published maps and institutional affiliations.



Open Access This article is licensed under a Creative Commons Attribution 4.0 International License, which permits use, sharing, adaptation, distribution and reproduction in any medium or format, as long as you give appropriate credit to the original author(s) and the source, provide a link to the Creative Commons license, and indicate if changes were made. The images or other third party material in this article are included in the article's Creative Commons license, unless indicated otherwise in a credit line to the material. If material is not included in the article's Creative Commons license and your intended use is not permitted by statutory regulation or exceeds the permitted use, you will need to obtain permission directly from the copyright holder. To view a copy of this license, visit <http://creativecommons.org/licenses/by/4.0/>.

© The Author(s) 2017